

Collective decision making by embodied neural agents

Nicolas Coucke ^{a,b,c,d,*}, Mary Katherine Heinrich ^c, Axel Cleeremans^d, Marco Dorigo ^c and Guillaume Dumas ^{a,e,f}

^aPPSP Team, CHU Sainte Justine Azrieli Research Center, Université de Montréal, Montréal, Québec, Canada

^bMoral and Social Brain Lab, Department of Experimental Psychology, Universiteit Gent, Ghent, Belgium

^cIRIDIA, Université Libre de Bruxelles, Brussels, Belgium

^dConsciousness, Cognition and Computation Group, Université Libre de Bruxelles, Brussels, Belgium

^eMila—Quebec Artificial Intelligence Institute, Université de Montréal, Montréal, Québec, Canada

^fDepartment of Psychiatry and Addictology, University of Montréal, Montréal, Québec, Canada

*To whom correspondence should be addressed: Email: nicolas.coucke@ugent.be

Edited By Lilianne Mujica-Parodi

Abstract

Collective decision making using simple social interactions has been studied in many types of multiagent systems, including robot swarms and human social networks. However, existing multiagent studies have rarely modeled the neural dynamics that underlie sensorimotor coordination in embodied biological agents. In this study, we investigated collective decisions that resulted from sensorimotor coordination among agents with simple neural dynamics. We equipped our agents with a model of minimal neural dynamics based on the *coordination dynamics* framework, and embedded them in an environment with a stimulus gradient. In our single-agent setup, the decision between two stimulus sources depends solely on the coordination of the agent's neural dynamics with its environment. In our multiagent setup, that same decision also depends on the sensorimotor coordination between agents, via their simple social interactions. Our results show that the success of collective decisions depended on a balance of intra-agent, interagent, and agent–environment coupling, and we use these results to identify the influences of environmental factors on decision difficulty. More generally, our results illustrate how collective behaviors can be analyzed in terms of the neural dynamics of the participating agents. This can contribute to ongoing developments in neuro-AI and self-organized multiagent systems.

Keywords: neuroAI, neurodynamics, multiagent, collective decision making, swarm intelligence

Significance Statement

Collective behaviors require the spatial and temporal coordination of actions by many individuals. The neural mechanisms that enable such coordination among embodied biological agents are not often considered. By using simulations of simple embodied agents equipped with biologically plausible neural dynamics, we demonstrated how collective decision making can result from adaptive coupling between an agent's neural dynamics, its environment, and other agents. Our approach provides a way to include intrinsic neural dynamics in multiagent systems, as a means to expand their ability for social interactions and collective tasks.

Introduction

Collective decision making is important to the normal functioning of human and animal groups (1, 2), and is also used in groups of artificial agents such as robots (3–5). Decisions can refer to physical actions, such as the direction of movement of animal groups (6), or symbolic questions that are disconnected from physical situations, such as those studied in collective estimation tasks in humans (7, 8). Collective decisions that are made by the group itself without external intervention typically require that a consensus emerge in the group. Consensus entails that all or at least a large majority of individuals agree, either on an approximate continuous value (e.g. a position in continuous space (9, 10)) or a discrete option (e.g. voting for an arbitrary item from a list (11)).

Consensus is achieved through a distributed process that is not under the control of any single agent (5). Multiagent models have been instrumental in investigating how the distributed interactions of individuals can result in a consensus. The individual agents used in most models behave according to rather simple rules or heuristics. For example, in the well-known “opinion dynamics” models, agents typically update their opinion according to the majority or to the voter rule (12–14). Some recent models aim to replicate human cognitive processes more closely by using neuro-inspired approaches such as the drift-diffusion model (15–18). These opinion dynamics models have greatly advanced our understanding of how peer-to-peer interactions can give rise to collective phenomena such as polarization or consensus.

Competing Interest: The authors declare no competing interests.

Received: August 22, 2024. **Accepted:** March 6, 2025

© The Author(s) 2025. Published by Oxford University Press on behalf of National Academy of Sciences. This is an Open Access article distributed under the terms of the Creative Commons Attribution-NonCommercial License (<https://creativecommons.org/licenses/by-nc/4.0/>), which permits non-commercial re-use, distribution, and reproduction in any medium, provided the original work is properly cited. For commercial re-use, please contact reprints@oup.com for reprints and translation rights for reprints. All other permissions can be obtained through our RightsLink service via the Permissions link on the article page on our site—for further information please contact journals.permissions@oup.com.

Another class of multiagent models addresses collective dynamics in physical space rather than opinion space (19). Such models pertain to, for example, animals choosing a new nest site or humans finding an exit during an emergency evacuation (20–22). Also, in these more embodied models, behaviors are typically governed by simple rules or heuristics (9, 23). These models have illuminated, for example, how animals can resolve differences in initial movement directions and move to a single location using only local, implicit communication.

The simple behavioral rules that agents use in these models are approximations of more elaborate brain processes that underlie behavior in biological organisms. Thanks to recent advances in multibrain neuroscience, it is now possible to simultaneously measure the brain activity of multiple interacting agents during collective behaviors (24). Despite these innovations, it remains unclear how the combined neural activity of multiple agents is involved in producing collective behavior. Computational models can be of help, by simulating how certain patterns of neural activity across agents produce collective behaviors (25). However, current multibrain models typically do not link the neural activity of agents to their behavior in an environment; so far, only a handful of multiagent models use brain-inspired mechanisms rather than simple heuristics to generate collective movements (26–28). In this study, we propose a multiagent model of collective decision making by embodied agents that are controlled by an oscillatory model of brain dynamics. Our goal with this approach is to pave the way for computational approaches that bridge neuroscience and the burgeoning field of collective behavior.

Considerations of the brain–body–environment interplay have gradually permeated cognitive science, culminating in the *4E cognition framework*, which sees cognitive processes as being embodied, enactive, embedded, and extended (29, 30). Similar considerations have become increasingly common in computational neuroscience and artificial intelligence research (31, 32). Largely inspired by the enactive approach to embodied cognition, we constructed minimalist agents that simulate important attributes of biological agents: (i) intrinsic neural dynamics produced autonomously by the agent and (ii) a constant sensorimotor loop with the environment (33–35). We studied how such agents can reach a consensus by continuously adjusting to one another's movements in a simple environment. We are not proposing that other approaches to modeling collective decision making are invalid. Rather, we wish to complement prior approaches, by providing a way of incorporating important and understudied aspects of embodied cognitive processes.

In order to successfully operate in an environment, the neural activity of a biological agent must be attuned to the characteristics of that environment. In neuroscience, brain activity is typically studied in terms of oscillations. Neural oscillations (also referred to as brain rhythms) have been linked to perception, movement, and even abstract cognition (36, 37). Across taxa, evolution has selected a subset of rhythms that allow organisms to adequately interact with their environment (38). Moreover, brain rhythms can rapidly shift to accommodate changing environments and task demands (39, 40).

Large-scale brain rhythms are produced by the coordinated oscillatory activity of many interacting brain regions. The *coordination dynamics* framework has been widely used to study how the activity of these dynamically interacting components is coordinated (41–43). One important advantage of the coordination dynamics approach is that it can be used to study the metastable regime in which the brain usually operates (44). If coordination

among brain regions were always stable, its dynamics could not be adequately modulated by the environment so as to allow the agent to engage in any adaptive behavior. On the other hand, overly unstable dynamics would result in the brain being too easily overwhelmed by environmental input, again preventing adaptive behavior. A metastable regime resolves this problem by allowing the brain to dynamically switch between several stable oscillatory states, thereby being neither completely stable nor completely unstable.

The Haken–Kelso–Bunz (HKB) equations provide a straightforward way to model metastable dynamics among interacting components, such as two populations of oscillating neurons in the brain (42, 45). Two oscillating components, when modeled with the HKB equations, show in-phase attraction (similar to the Kuramoto model (46)) and also antiphase attraction. The simultaneous existence of in-phase (symmetrical) and antiphase (asymmetrical) attraction produces a simple form of metastability (47). The HKB equations were first implemented as a neural controller of an embodied agent by Aguilera et al. (48), to model the sensorimotor interactions of a situated agent with its environment. The authors illustrated the importance of taking into account embodied interactions when studying brain dynamics, by showing that the simulated neural dynamics of the agent were qualitatively different when sensorimotor interactions with the environment were disrupted. In this study, we adopted the HKB agent of Aguilera et al. (48) and modified it so that it could support embodied collective decision making. By making our agent sensitive to both the environment and other agents, we could study the oscillatory neural dynamics of agents when coordinating with both each other and the environment.

In studies of continuous collective decision making, an often-studied question is: under which conditions can agents with different preferred movement directions reach a consensus? For example, two influential modeling approaches have shown that reaching a consensus is facilitated by the presence of a subgroup of unopinionated individuals (9, 49). In this study, we investigated how this ability to reach consensus is modulated by the agents' neural dynamics. In line with the enactive approach to embodied cognition, we expected that an agent can operate in its environment when it balances (i) its intrinsic neural activity with (ii) its sensorimotor coordination with the environment. To investigate this, we first assessed how a single agent's movement towards one of two local optima in its environment depended on the relative strength of the internal coupling of its brain oscillators versus its coupling to the environment. Agents involved in collective decisions must additionally balance interaction with other agents. Therefore, when we embedded a group of agents with varying initial states in an environment, we assessed how the success of collective decisions depended on a balance of not only intra-agent and agent–environment coupling but also interagent coupling (i.e. social influence). Lastly, we connected our model to previous models of collective decision making, by assessing how consensus is influenced by differences in (i) the quality of the two stimulus sources in the environment and (ii) differences in individuals' initial states.

Model

Task environment

We created a simple environment in which agents could move and sense a stimulus. The environment contained one or more stimulus sources (i.e. sites), at which stimulus concentration is maximal (Fig. 1B and C). The stimulus concentration in the

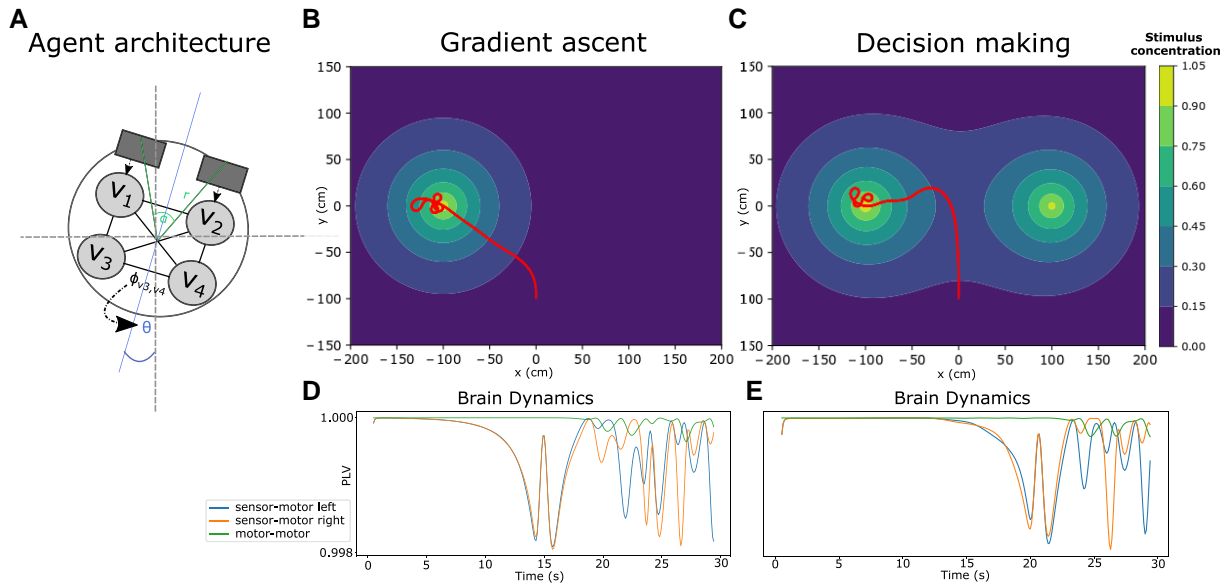


Fig. 1. Single-agent behavior and neural dynamics. A) The agent architecture: two sensors, each connected to a sensory oscillator, nodes 1 and 2 (v_1 and v_2), that are each in turn connected to a motor oscillator, nodes 3 and 4 (v_3 and v_4). The traveling orientation θ of the agent is determined by the angle difference ϕ_{v_3, v_4} between motor oscillators. B) Gradient ascent: the agent's trajectory in the environment (brighter colors indicate higher stimulus concentration). C) Decision making: two stimulus sources are present in the environment and the agent's performance is measured by its ability to approach one of the two. D) Internal phase locking of oscillators (contralateral sensor-motor and motor-motor) in (B). E) Internal phase locking of oscillators in (C).

environment was inversely proportional to the distance from the stimulus source. Thus, the stimulus concentration followed a gradient from low to high concentration when approaching the stimulus source. A simple task that agents could perform in this environment was that of gradient ascent, i.e. following the gradient towards maximal stimulus concentration (Fig. 1B) (48). If one imagines the stimulus as “light,” and the stimulus source as a light source, then this behavior is reminiscent of the light-seeking behavior of organisms such as fireflies (50) or zebrafish (51). When two sources of stimulus are present, the scenario could be considered a binary decision-making task (Fig. 1C). In this scenario, an agent could successfully reach a stimulus source if it could “decide” between the two sources. In the multi-agent scenario, the task became a collective binary decision-making task. In this scenario, 10 agents started at the same position, but had different initial orientations (Fig. 2B). Due to these different initial orientations, agents could end up at different sites (Fig. 2C). However, agents had some social information about each other's position (Fig. 2A; see below), and their task was to use this information to aggregate at the same site. We quantified performance of collective decision making according to how closely the agents collectively approached a single candidate site (see Methods).

Agent

We modeled an agent with minimal neural dynamics that could use sensorimotor coordination with the stimulus sources and the movements of other agents in order to move towards a candidate site. Our agent architecture was based on a minimal Braitenberg vehicle (52), which is a self-driven agent with a very simple architecture: two sensors directly control two motors. To give our agent intrinsic neural dynamics, we connected two oscillator nodes to the sensors (loosely representing sensory brain regions; nodes 1 and 2 in Fig. 1A) and two oscillator nodes

connected to the direction of the movement of the agent (loosely representing motor regions; nodes 3 and 4 in Fig. 1A). This design resembles the *situated HKB agent* of Aguilera et al. (48), which had two oscillator nodes (one sensory and one motor). Our agents have four nodes, so that they can use stereovision and differential drive to move directly to a stimulus source, rather than approaching it in a spiraling motion (cf. (48)).

To model the interaction between the oscillators, we used an update rule for the phase of each oscillator, based on the following version of the HKB equation (53):

$$\dot{\phi}_{v_i} = \delta \omega_{v_i} + c I_{v_i} - \sum_{j=0}^N a_{v_i, v_j} \sin \phi_{v_i, v_j} - \sum_{j=0}^N b_{v_i, v_j} \sin 2\phi_{v_i, v_j}, \quad (1)$$

where ϕ_i is the phase change of node v_i , and ω_{v_i} is the intrinsic frequency of oscillator v_i . Parameters a_{v_i, v_j} and b_{v_i, v_j} represent the contribution of, respectively, in-phase attraction, and antiphase attraction between oscillators v_i and v_j . Lastly, c parameterizes how strongly the oscillator phase is modulated by sensory input I_{v_i} . This parameter is set to zero for each motor oscillator, because it is not connected to a sensor. (See Methods for the version of the update equation used for each oscillator.)

Our agent moves at a constant speed and the activity of the motor oscillations is linked to the agent's movement direction. The heading is updated according to the phase angle between the two motor oscillators, such that

$$\dot{\theta} = \eta \phi_{v_3, v_4}, \quad (2)$$

where θ is the orientation of the agent in the environment and η is a scaling factor. Together, these equations create a closed sensorimotor loop between the agent's internal oscillator dynamics and the external environment.

In the multiagent scenario, we gave agents the added behavior of emitting the same stimulus that they observed to be present in

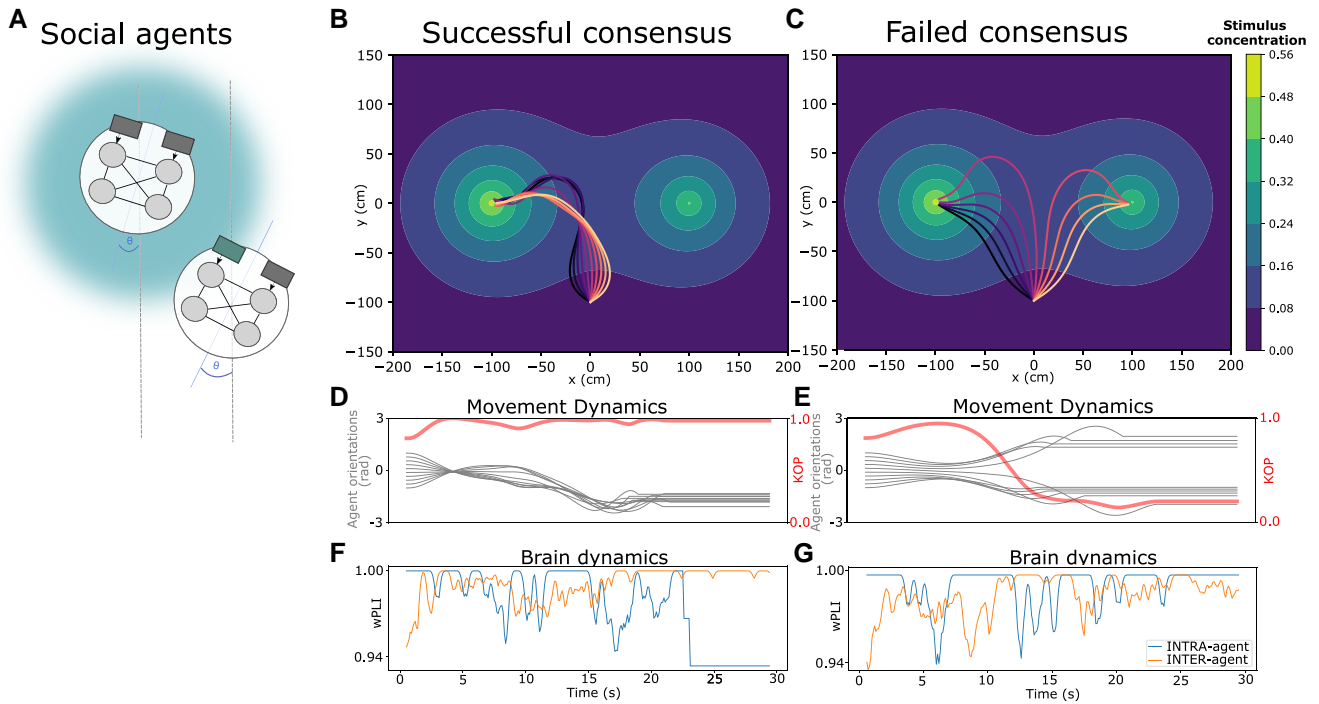


Fig. 2. Agent behavior and intra-agent neural dynamics during collective decision making. A) Agents emit stimulus that can be perceived by other agents. B) Higher social stimulation allows agents to converge onto the same stimulus source in their environment. C) With lower social stimulation, agents do not converge on the same source. D and E) Movement angles of agents (thin lines) and KOP of the group, indicating the degree of alignment (thick line). Alignment increases when all agents are moving towards the same stimulus source and decreases when they are not. F and G) Intra- and interagent neural dynamics: average intra-agent wPLI and average interagent wPLI.

the environment. The stimulus concentration emitted by social agent j was perceived by agent i as:

$$I_{ij} = S * e^{-\lambda_a D_{ij}}, \quad (3)$$

where D_{ij} is the Euclidean distance between agent i and agent j , S is the strength of social influence between agents (identical for all agents), and λ_a is the decay rate of the emitted stimulus. Note that an agent did not perceive its own emitted stimulus. This reflects the attenuation of self-produced stimuli in many animal species (54, 55).

Results

We performed both single-agent simulations and multi-agent simulations. For the single-agent simulations, we quantified neural coordination dynamics in terms of integration and metastability. The integration of brain regions by means of phase-locked activity is a central mechanism of brain function (56, 57), and can be quantified using the phase-locking value (PLV), see Section 'Measures of coordination dynamics'. Brain function supportive of adaptive behavior relies on switching between different brain states. To quantify this aspect of neural dynamics, we used the standard deviation of the Kuramoto order parameter SD(KOP) (58, 59), see Section 'Measures of coordination dynamics'.

For the multiagent simulations, we additionally quantified the coordination dynamics occurring across the different agents. We analyzed agents' movement trajectories using the KOP as a measure of alignment, and SD(KOP) as a measure of alignment variability between agents' movements (58, 59). Lastly, we also quantified the degree of coordinated activity between the neural dynamics of the different agents by using the weighted phase-lag index (wPLI), a measure of phase locking that discards zero-phase coupling and

can be interpreted as the co-variance between two signals (60), see Section 'Measures of coordination dynamics'.

Single-agent simulations

We first performed a series of single-agent simulations to assess how an individual agent's neural dynamics are related to its ability to move towards a stimulus source in its environment. In the single-agent setup (see Fig. 1), an agent tried to climb a gradient towards a global maximum. To simulate different types of neural dynamics, we varied the internal coupling strength between the agent's oscillator nodes (a_{v_i, v_j} in Eq. 1), and varied whether or not it was sensitive to external stimuli. For each agent configuration, we performed 50 runs with different random initial oscillator phases. In Fig. 3, we characterize the neural dynamics associated with each agent configuration. The top panel shows the average level of integration (i.e. phase locking) between the agent's oscillators, measured by the mean PLV, and the bottom panel shows the degree of metastability among the agent's oscillators (measured by SD(KOP); see Methods).

It is notable that, in the absence of sensory input, the system quickly found a stable state with minimal variation in oscillator dynamics: agents without stimulus input (squares in Fig. 3) consistently had values close to PLV = 1 and SD(KOP) = 0. Conversely, agents with sensory input (circles in Fig. 3) had a broad range of parameter values that resulted in lower PLV and higher SD(KOP). This shows that, as expected, sensory input can alter the coordination regime of the neural dynamics. In the presence of sensory input, PLV decreases as internal coupling increases from 0 to 1, indicating that the neural dynamics at low internal coupling are mostly driven by stimulus input, without being significantly modulated by the interactions among the agent's own oscillators. Simultaneously, SD(KOP) remained relatively high, indicating that, at low internal

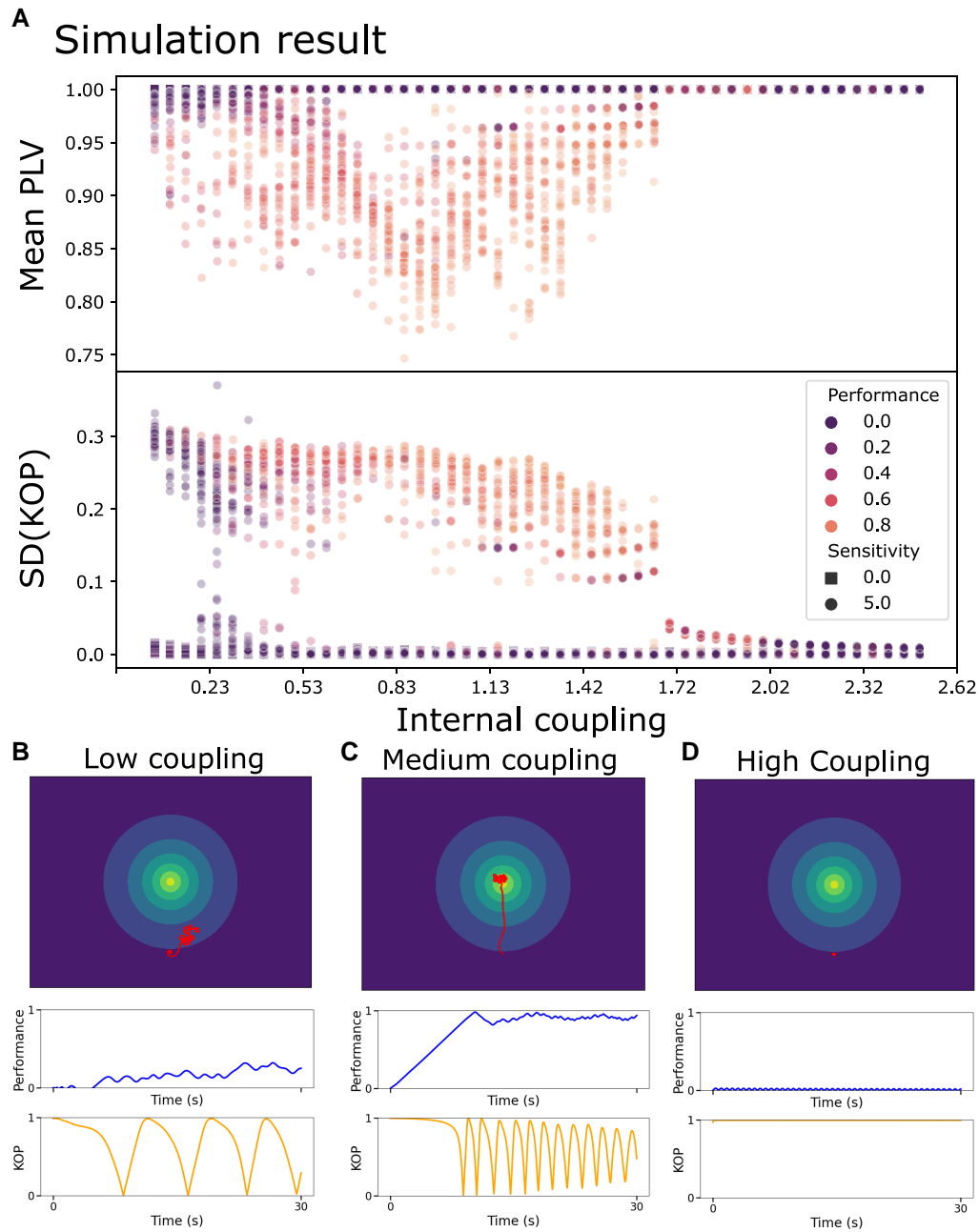


Fig. 3. A) Intra-agent neural dynamics: the mean PLV and SD(KOP) of each agent during its run (y-axis), according to the internal coupling degree in its neural controller (x-axis). The values on the x axes represent the strength of in-phase coupling (a_{v_i, v_j}); antiphase coupling (b_{v_i, v_j}) was always set to $0.5 \cdot a_{v_i, v_j}$. Squares represent agents without sensory input and dots represent agents with sensory input. Lighter colors represent higher performance. For each configuration (i.e. internal coupling degree and stimulus sensitivity), 50 runs were performed with random initial phases of the oscillators. Each data point represents the average of one run. B–D) Trajectories at low ($a_{v_i, v_j} = 0.1$), medium ($a_{v_i, v_j} = 1.1$), and high ($a_{v_i, v_j} = 2.2$) internal coupling. Upper panels represent the agent trajectory during one trial. Middle panels represent performance (degree to which agent reaches the stimulus maximum) during that same trial. The bottom panels represent the KOP during the trial.

coupling, sensory input caused the system of oscillators to quickly cycle between oscillatory states.

As the agent's internal coupling increases further, the interactions between the agent's oscillators become strong enough to meaningfully modulate sensory input, which results in a lower level of apparent oscillator integration, with PLV decreasing to 0.75 while the degree of metastability plateaus. Beyond an internal coupling level of $a_{v_i, v_j} = 1.4$, the internal coupling of the agent's oscillators started to dominate, which resulted in highly integrated oscillators, indicated by higher PLV. At an internal coupling level

of $a_{v_i, v_j} = 1.7$, the effect of internal coupling became strong enough that it nullified the effect of any sensory input, resulting in PLV = 1 (indicating no variation in inter-oscillator dynamics). This increase in integration was accompanied by a sharp drop in metastability, indicating that the system tends to get stuck in a single stable state. Such a stable state of high integration between oscillators precludes changes in movement direction in response to sensory input, inhibiting the agent from approaching the stimulus source.

The colors of the data points in Fig. 3 indicate agent performance: brighter colors indicate that the agent was better able to

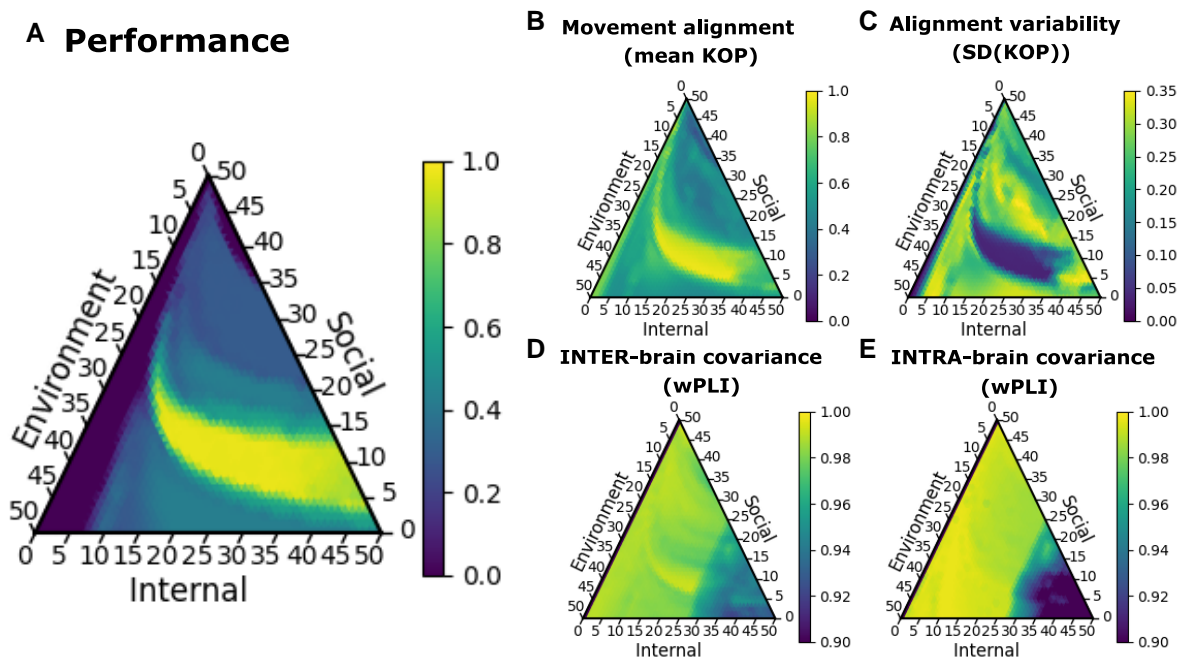


Fig. 4. Ternary plots illustrating how collective behavior and neural dynamics depend on the agent configuration. Each point in the triangle corresponds to a certain weighting of environmental stimulus, social information, and internal motor coupling. In each simulation, the parameters fulfill the condition stimulus sensitivity + social sensitivity + internal coupling = 100. The scale [0, 50] for each dimension corresponds to respective parameter values of $c \in \{0, \dots, 10\}$ for stimulus sensitivity, $S \in \{0, \dots, 5\}$ for social sensitivity, and $a_{v_3, v_4} \in \{0, \dots, 1\}$ for internal coupling. The top corner corresponds to maximal social sensitivity, the left corner to maximal environmental sensitivity, and the right corner to maximal internal coupling. The brightness (yellowness) in panel A) indicates the performance of collective decision making. A performance of 0 indicates that agents failed to reach either of the two stimulus sources. A performance of 0.5 indicates that half of the agents reached the same stimulus source. A performance of 1 indicates that all agents reached the same stimulus source and thus that a consensus was reached. The brightness in panels B)–E) indicate the strength of, respectively, the movement alignment, alignment variability, inter-brain covariance, and intra-brain covariance.

approach the stimulus. The distribution of colors shows that agents performed best in the range $a_{v_i, v_j} \in \{0.8, \dots, 1.5\}$. At these intermediate coupling values, there was a decrease in oscillator integration (as shown by PLV) and moderately high metastability (as shown by SD(KOP)). In short, these results show that at low internal coupling, neural dynamics are mostly driven by sensory input, and the oscillatory coordination states do not enable the agent to maintain a coherent travel direction (Fig. 3B). At moderate internal coupling, neural dynamics modulate sensory input without fully dominating it. In this intermediate range with relatively low integration and high metastability, the agent displays adaptive behavior. For example, Fig. 3C shows how oscillators are initially largely in sync while the agent travels up the gradient, and metastability allows the agent to approach the maximum. At high internal coupling, neural dynamics nullify the effect of sensory input and agent behavior cannot change in response to the environment (Fig. 3C). (See the [supplementary, text S2](#) for a more elaborate analysis of gradient climbing and decision making by single agents, as well as its relation to neural dynamics.)

Multiagent simulations

We ran two sets of multiagent simulations. In the first set of simulations, we varied parameters related to the agent configuration (internal coupling, environmental sensitivity, and social influence) and observed the effects on decision-making performance and collective dynamics. In the second series of experiments, we kept the agent configuration constant and modified the quality difference between the two stimulus sources in their environment, as well as the starting angles between the agents.

Consensus as a function of internal, environmental, and social influences

We conducted a series of simulations with groups of 10 agents in an environment with a fixed quality (brightness) ratio of $r = 0.8$ between the two stimulus sources (Fig. 2). For each simulation run, we quantified the performance as the degree to which agents could approach the same stimulus source (as in Fig. 2B) rather than going to different sources (as in Fig. 2C; see Methods). Throughout each simulation, we track the coordination dynamics among agents' movements (Fig. 2D and E), as well as measures of coordination between the neural dynamics of the different agents (Fig. 2G and H).

We conducted simulations for different parameter values of internal coupling strength (a_{v_i, v_j} in Eq. 1), sensitivity to the environment (c in Eq. 1), and the degree of social influence (S in Eq. 3). For each combination of parameter values, we display the final performance in a ternary plot (Fig. 4A). Each of the three corners of the ternary plot corresponds to one of the parameters being maximal and the others zero. We also display the corresponding measures of movement coordination and neural coordination dynamics for each parameter combination in adjacent plots (Fig. 4B–E).

We assessed movement coordination in terms of the movement alignment (KOP) and the variability in movement alignment (i.e. "alignment variability"; SD[KOP]). To assess the coordination dynamics within and between agents' neural dynamics, we used a measure of phase covariance (wPLI), rather than the PLV used for the single-agent case. In contrast to the PLV, the wPLI does not take into account zero-lag coupling between oscillators. Measures with this property are preferred in multibrain neuroscience, since

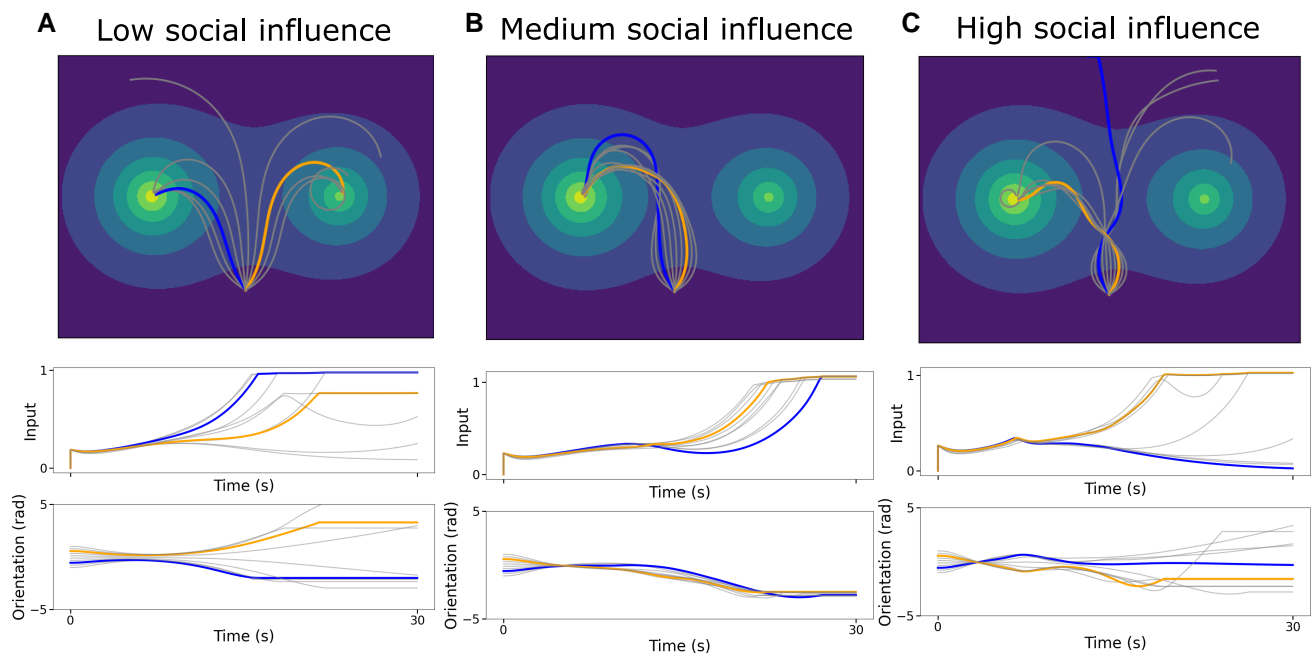


Fig. 5. Illustration of agent trajectories, stimulus input for each agent, and orientation (output) each agent. In panel A), agents experience low social influence ($S = 1.1$), medium influence ($S = 1.6$) in panel B), and high influence ($S = 2.4$) in panel C). The upper row of plots shows agent trajectories during one trial. The middle row shows the stimulus experienced by each agent during that same trial. The bottom row shows each agent's orientation during that trial. In each panel, the trajectories of two focal agents during one trial are highlighted.

they discount spurious coordination due to, e.g. common input from the environment (61, 62). In our simulations, spurious coordination between oscillators could similarly have been caused by identical initial phases of agents' oscillators (see Methods).

The middle region of the plots in Fig. 4 corresponds to a parameter range in which internal, environmental, and social influences are appropriately balanced for reaching consensus, as indicated by the bright yellow area in Fig. 4A. This region was accompanied by high movement alignment and low alignment variability, indicating that agents could use environmental and social information to coherently move towards the same stimulus source. Part of this region corresponds to a narrow area of increased inter-brain covariance, indicating that this aligned movement was accompanied by coordinated neural dynamics across agents. The lower right corner of the plots corresponds to a region of increased internal influences and decreased social influences. As long as social influences are nonzero, performance remains relatively high in this parameter range. Movement alignment is decreased and alignment variability is increased relative to the middle part of the plot. This indicates that, when internal coupling increases, agents' movements become less aligned, but can still result in consensus. Interestingly, the lower right corner of the plot corresponds to a decrease in both intra-brain covariance (between different oscillator nodes within the same agent) and inter-brain covariance (between the same oscillator nodes across different agents). More alignment variability among the agents' movements is thus accompanied by brain dynamics that are more independent.

A last and interesting observation in Fig. 4 can be made at the left edge of the plots, where internal coupling is low. In this region, agents are driven entirely by a combination of social and environmental influences. This region in parameter space was accompanied by high movement alignment and low alignment variability, but was associated with a decrease in performance. This suggests that agents moved in a highly aligned manner, but failed to collectively approach either of the two stimulus sources. This outcome highlights the

importance of balancing external influences with sufficient internal coupling. When agents are overly coupled to external stimuli without enough counteracting internal coupling, they struggle to move towards an increasing stimulus concentration.

Figure 5 illustrates how some social influence can aid collective decision making, but too much social influence can prevent agents from reaching any option at all. At low social influence (Fig. 5A), agents are attracted to the stimulus that is in line with their original travel direction. At medium social influence (Fig. 5B), there is initially enough social influence to group the agents together before they come close to an option. At high levels of social influence (Fig. 5C), social influence can temporarily guide the movement direction of some agents so strongly that they steer away from any option. Figure S5 illustrates this phenomenon further.

Taken together, these results show that agents reach a consensus when their configuration facilitates a balanced integration of environmental, social, and internal influences, and this is reflected in neural and behavioral dynamics. The parameter values that are conducive to consensus are dependent on the initial starting positions and orientations of the agents (see [supplementary, section S4](#)).

Consensus as a function of environment configuration

If the ability to reach a consensus depended on the features of the environment, we would expect that binary decision making should be easier (and thus performance higher) when the difference between the two stimulus sources is larger, and when the initial angle between the agents is smaller. We performed simulations with 10 agents with a fixed architecture, and varied the initial starting angle between agents and the brightness ratio between the two stimulus sources (see Methods).

The results in Fig. 6 show that, overall, performance depended on a combination of starting angle and stimulus ratio. Performance was maximal when agents had identical starting orientations and only

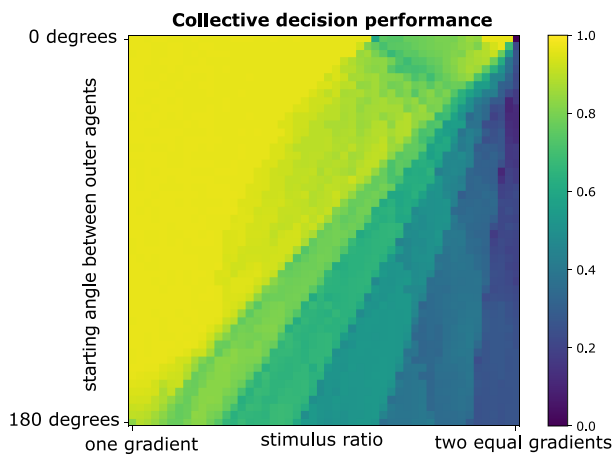


Fig. 6. Dependence of the collective decision-making performance on the environment and initial orientations of agents. The leftmost extreme of the x-axis represents the cases with only one stimulus source present in the environment. Moving towards the right, the brightness of a second stimulus source increases until the two have equal brightness. The agents always start with equal angles between them. At the bottom of the y-axis, the agents are spread so that the outermost two of the 10 agents are at a 180° angle. At the top of the y-axis, all agents start with angles of 0° between them. All agents have identical parameters; stimulus sensitivity is $c = 3$, social sensitivity is $S = 1$, and internal coupling is $a_{v_i, v_j} = 0.5$.

one stimulus source was present (top left of Fig. 6). In accordance with our expectations, performance decreases as the second stimulus source became brighter and the starting angle between agents increased.

It should be noted that performance did not increase linearly as the decision-making task became easier. Rather, there was a repeating pattern of sharp decreases in performance followed by short plateaus. This was most likely due to a combination of our performance measure and the relatively small number of agents (see Methods). Each drop in performance was caused by one of the ten agents moving away from the global maximum and towards the competing local maximum (i.e. to the stimulus source with lower brightness). Figure S3 provides a more detailed account of this pattern. Overall, these simulations show that the ease with which the agents reach a consensus depends not only on their architecture but also on the environment in which they operate.

Discussion

We have modeled collective decision making with embodied neural agents that are controlled by simple oscillatory brain dynamics. We first showed that the ability of an agent to move towards a stimulus source was reflected in the intra-brain dynamics of that agent. In an intermediate parameter range where agents were neither overwhelmed by environmental stimulus nor insensitive to it, neural dynamics could become sufficiently uncoupled and metastable to allow the agent to approach its target. Furthermore, multiple agents with different initial heading directions could overcome their differences and converge on one of the two available options. Agents were able to do this within a parameter range that adequately weighted environmental, social, and internal influences. When one influence was too high with respect to the others, the agents failed to converge on a decision. In this regard, our model differs from more disembodied multiagent models (14). In disembodied cognition models of collective decision making, increasing social influence to an arbitrarily high degree would lead to a fast and efficient convergence on any of

the possible decision options. The option selected may be of greater or lesser quality, but the ability of agents to reach any option at all has rarely been studied. Our results showed that, when increasing social sensitivity too much, the agent's neural dynamics may become saturated with social information—to such a degree that it cannot adequately interact with the environment and move towards one of the options. This is reminiscent of real-world situations in which agents that are too consumed by interacting socially with one another lose adaptive interactions with the environment (see Strasbourg dancing plague (63) or circular milling in army ants (64)). This example illustrates how our model can be used as one possible framework (among many) to examine how certain collective behaviors emerge.

Our model also differs from the more embodied multiagent models of movement-based collective decisions by animals. In most such models, agents have a parameter that explains their preferred target location or movement direction (6, 27, 49). In our simulations, agents had different initial movement directions but did not have a parameter representing a preferred movement direction. Rather, their movement direction emerged from their interactions with each other and with their environment. Our results showed that the more an agent's initial movement direction was between the two sources rather than pointing to one of them, the more likely agents were to reach a consensus. These results are somewhat in line with previous findings that a larger proportion of unopinionated individuals promotes consensus in models of movement-based decisions made by groups of animals? (6, 49).

Our simulations also showed that a larger difference between the quality of stimulus sources in the environment generally resulted in a higher proportion of agents reaching a consensus. This is in accordance with studies of discrete decision making between a few options in an environment, where models have shown how the speed and accuracy of collective decisions depend on differences between environmental stimuli (5, 65). Models that do not take into account the quality of options in the environment, or that consider options of equal quality, often observe agents traveling in a compromise direction (49). Since agents' neural dynamics were strongly influenced by the environment in our simulations, such compromises only occur in a small region of the parameter space. The closer agents came to a stimulus source, the higher the stimulus concentration they observed, causing agents to almost always go to one of the two stimulus sources instead of taking a compromise direction. Our simulations also showed some surprising emergent collective behaviors, such as “overshooting” in response to social influence and, as a result, moving towards an option that corresponds neither with the initial movement direction nor with the option chosen by other agents (see Fig. SSA).

In the current paper, we performed deterministic simulations of agents that started from the same position and moved towards one of two stimulus sources. In future work, our model could be studied in environments with a higher number of stimulus sources, without changes to the agent architecture (27). Furthermore, agents might be allowed to visit multiple options of stimulus sources before converging on one, as is common in collective decisions of ants and honeybees (22, 66). In this setting, it might be interesting to let the social stimulus emitted by the agents decay more slowly (instead of instantaneously), allowing the agents to influence each other asynchronously. Such *stigmergic* coordination is often observed in social insects such as ants (67). Another extension of our simulations could be to let agents start from different spatial locations. Using the HKB equations to maintain asymmetric patterns of coordination between different agents' oscillators, future work could study a rudimentary allocentric way of using social

information (68). Future work could also study the influence of noise on collective performance of embodied neural agents, especially in environments with many local optima, as random fluctuations are often an important aspect of self-organized systems and collective intelligence (69, 70).

Inspired by the brain dynamics of biological agents, we used oscillator models to study neural dynamics in a multiagent system. Recent *swarmalator* models have also combined collective movement with oscillator dynamics (71, 72). In these models, an agent's behavior is based on the directly observed oscillator phases of the surrounding agents. In our model, the oscillators represent brain dynamics that are not directly available to an outside observer. The brain dynamics of the agents can only become coordinated by intermediary of their behavior. Moreover, since the stimulus emitted by agents was indistinguishable from stimulus originating in the environment, agents could not selectively react to instantaneous social stimulation. Yet, agents could interact by mutually reacting to local changes in stimulus concentration caused by their respective movements in the environment. This situation reflects a form of social interaction in which agents cannot use any social cognition capabilities other than those involved in the interaction itself. Such situations are also studied with human participants in perceptual crossing experiments, and have led some to argue that social interaction can be constitutive of social cognition (73, 74).

Using oscillators to model brain dynamics allows us to use phase-locking and phase-covariance measures to quantify the degree of coordination between the brain dynamics of different agents (61). Experimental studies with multiple animals or humans have suggested that coordination between brain dynamics of different agents, typically quantified in terms of inter-brain synchronization (IBS), might have an important role in supporting collective behaviors (75, 76). A few computational models have provided initial mechanistic explanations for the emergence of such inter-brain synchrony by using the Kuramoto model, showing that the strength and frequencies at which IBS takes place depend on a combination of agents' individual brain dynamics and their interagent coupling (77, 78). Although our results cannot conclusively show whether collective decision-making performance depended on interagent synchrony, our models could provide a way to study the complex brain-brain behavior dynamics that can give rise to IBS. Furthermore, our results replicate an interesting finding of Kuramoto models of interpersonal synchrony, namely that some degree of intra-agent coupling is required to achieve rich patterns of interpersonal coordination (79). While previous studies (e.g. (79)) have shown this requirement when a pair of agents were coupled to each other directly, we have confirmed it for multiple agents embedded in a spatial environment.

A major challenge in the development of artificial agents is coordinating social interactions with both humans and other artificial agents. Recent developments in Social NeuroAI attempt to bring social interaction into the realm of AI by advancing artificial agents' social embodiment, temporal dynamics, and biological plausibility (80). In this work, we accommodate (i) social embodiment, as collective decisions are movement-based and agents can be reciprocally influenced by each other's movements; (ii) temporal dynamics, through continuous intra-agent, interagent, and agent-environment interactions; and (iii) biological plausibility, by using oscillations to control agent behavior. Our approach could be a starting point for developing social-neural agents that collaborate on a wider range of collective tasks through the implicit coordination of their neural dynamics.

Methods

Experiment setup

Each experiment took place in a 2D environment in which every position had an associated stimulus concentration. Depending on the experiment type, each environment contained one or more stimulus sources of different quality. The stimulus concentration at a certain position was exponentially proportional to its closeness to the stimulus source:

$$I(x, y) = e^{-\lambda D(x, y)}, \quad (4)$$

where $D(x, y)$ is the Euclidean distance to the stimulus source and $\lambda = 0.02$ is the exponential decay rate of the environmental stimulus. In setups with two stimulus sources, each had stimulus concentrations defined by Eq. 4, and the overall stimulus concentration at a certain position was the combination of the two:

$$I(x, y) = e^{-\lambda D_1(x, y)} + r e^{-\lambda D_2(x, y)}, \quad (5)$$

where r indicates the quality ratio of the two stimulus sources. When there were multiple agents in an environment, the stimulus level that an agent perceived was a combination of the stimulus concentration in the environment and the stimuli concentrations emitted by other agents, such that

$$I_i(x, y) = e^{-\lambda D_1(x, y)} + r e^{-\lambda D_2(x, y)} + S \sum_j e^{-\lambda_s D_{ij}}. \quad (6)$$

In all experiments, the environment was 300 by 400 cm, the radius of each agent's body was 2.5 cm, and each agent has a fixed velocity of 10 cm/s. Simulations were performed with a timestep of 0.01 s. All experiments ended after 30 s, which provided sufficient time for agents to reach a stimulus source in the environment. All simulations were performed in Python version 3.9.2 (81), and the agents were implemented in Pytorch version 1.12.0 (82).

Agent design

In our agents, sensory input did not directly control motor activity. Sensory information (in the form of stimulus concentration) was first integrated into the oscillator phase of two sensory nodes. These sensory nodes were dynamically connected to two motor nodes.

The situated agent designed by Aguilera et al. (48) consisted of one motor oscillator and one sensory oscillator, and thus could only perform gradient ascent with spiraling movement. We resolved this by giving our agent two sensory oscillators for stereovision (v_1 and v_2 , see nodes 1 and 2 in Fig. 1A) and two motor oscillators for differential drive steering (v_3 and v_4 , see nodes 3 and 4 in Fig. 1A). The sensors are directionless and are placed at the front of the agent, 90° apart as measured from the agent's center (see Fig. 1A). The orientation θ of the agent in the environment is determined by the angle between the two motor oscillators (v_3 and v_4 , see nodes 3 and 4 in Fig. 1A).

Altogether, the dynamics of the agent are governed by the following set of equations:

$$\dot{\phi} \begin{cases} \phi_{v_1} = \omega_{v_1} + cI_l - \sum_j a_{v_1, v_j} \sin \phi_{v_1, v_j} - \sum_j b_{v_1, v_j} \sin 2\phi_{v_1, v_j}, \\ \phi_{v_2} = \omega_{v_2} + cI_r - \sum_j a_{v_2, v_j} \sin \phi_{v_2, v_j} - \sum_j b_{v_2, v_j} \sin 2\phi_{v_2, v_j}, \\ \phi_{v_3} = \omega_{v_3} - \sum_j a_{v_3, v_j} \sin \phi_{v_3, v_j} - \sum_j b_{v_3, v_j} \sin 2\phi_{v_3, v_j}, \\ \phi_{v_4} = \omega_{v_4} - \sum_j a_{v_4, v_j} \sin \phi_{v_4, v_j} - \sum_j b_{v_4, v_j} \sin 2\phi_{v_4, v_j} \end{cases} \quad (7)$$

$$\dot{\theta} = \eta \phi_{v_3, v_4} = \eta (\phi_{v_3} - \phi_{v_4}), \quad (8)$$

where we fixed the ratio $k = \frac{b}{a} = 2$ so that the HKB equations are bistable (see [supplementary, text S1](#)).

In our neural controller, the oscillators influenced each other over the following connections: the contralateral ones ($a_{v_1, v_4} = a_{v_4, v_1}$ and $a_{v_2, v_3} = a_{v_3, v_2}$) the one between the motor regions ($a_{v_3, v_4} = a_{v_4, v_3}$), as well as their antiphase counterparts. Thus, we kept the two sensory oscillators independent and incorporated the contralateral sensorimotor connections present in the Braitenberg vehicles (52) and in many of the biological neural organizations (83). The intrinsic frequencies of all oscillators were set to 5 Hz, to resemble the frequency of the theta oscillations in biological brains. In our model, the next phase of each oscillator is calculated at each time step, by integrating the differential equations using the fourth-order Runge–Kutta method.

Single-agent experiments

In the single-agent gradient ascent setup, the agent initiated movement at xy position (0, −100) and the stimulus source was located at xy position (−100, 0). To study the link between a single agent's behavior and its intra-agent neural dynamics, we varied the sensory sensitivity ($c = 0$ or 5, in Eq. 7) and the coupling strength of all connections (a_{v_i, v_j} values from 0.05 to 2.5, in steps of 0.05, in Eq. 7). For each variation combination, we performed 50 runs with random initial phases of the oscillators.

In the single-agent binary decision making setup, the first stimulus source was located at xy position (−100, 0), the second at xy position (100, 0), and the brightness (i.e. quality) ratio of the two stimulus sources is $r = 0.95$ (see Eq. 6). The agent initiated movement equidistant to the two stimulus sources, at xy position (0, −100) with all internal oscillators starting as in-phase. To evaluate the dependence of performance on agent behavior, we varied the stimulus sensitivity of the agent (c values from 0 to 10, in steps of 1, in Eq. 7) and the internal coupling (a_{v_i, v_j} values from 0.05 to 2.5, in steps of 0.05, in Eq. 7). To evaluate the importance of internal coupling, we also varied whether the motor regions were connected or not ($a_{v_3, v_4} = 0$, in Eq. 7). We ran one simulation for each variation combination, since we did not introduce an element of randomness in the simulation.

Multiagent experiments

Each multiagent experiment had a group of 10 agents and an environment with two stimulus sources, located at xy positions (−100, 0) and (100, 0). To study consensus achievement under divergent starting opinions, we evenly distributed the initial orientations of the agents (between angle $-\theta_{\max}$ and θ_{\max} , $\theta_{\max} \in [0^\circ, 180^\circ]$). Thus, each agent faced a different initial direction, with half facing more towards the left-hand stimulus source and half facing more towards the right-hand one. Following (49, 84), the agent behavior in these experiments was deliberately deterministic. Although noise can be highly beneficial to the self-organization of complex systems (70), our focus in this study was specifically on the relationship between interagent dynamics and consensus, rather than exploring how noise might modulate these dynamics. Physical collisions were not considered in these simulations: agents only reacted to stimulus; their bodies could not collide with one another.

We ran two groups of multiagent experiments. In the first group, to study the influence of the intra- and interagent coordination regimes, we varied the degree of internal coupling between the motor oscillators (a_{v_i, v_j} values from 0 to 1, in steps of 0.02, in Eq. 7), the social sensitivity (S values from 0 to 5, in steps of 0.1, in Eq. 3), and the stimulus sensitivity (c values from 0 and 10, in steps of 0.5, in Eq. 7). In these experiments, the starting angle between agents was 10° and the brightness (i.e. quality) ratio of the two stimulus sources was $r = 0.8$. This ratio is lower than that in the

single-agent case, to facilitate a wider range of collective behaviors. With a higher ratio, agents initially oriented towards the least bright stimulus source did not deviate enough from their initial movement path for collective dynamics to occur.

In the second group, to study the influence of the environmental and initial conditions, we varied the brightness (i.e. quality) ratio of the two stimulus sources (r values from 0 to 1, in steps of 0.02) and the starting angles of the agents (from 0° to 18° , in steps of 0.36°). In these experiments, the stimulus sensitivity was $c = 3$, social sensitivity is $S = 1$, and internal connection was $a_{v_i, v_j} = 0.5$.

Evaluation

In single-agent setups, performance is based on the agent's end position relative to a stimulus source. Note that, in these experiments, the agent could continue moving after reaching a source, so the performance metric includes how well the agent remained close to a source after initially approaching it. For gradient ascent, we evaluated performance based on how closely the agent approaches the stimulus source:

$$\text{performance} = 1 - \frac{D(t_{\text{end}})}{D(t_0)}, \quad (9)$$

where $D(t_0)$ and $D(t_{\text{end}})$ represent the agent's distance to the stimulus source at the beginning and end of the simulation. For binary decision making, we evaluate how closely the agent approaches its closest stimulus source, regardless of the source's brightness level:

$$\text{performance} = 1 - \frac{\min\{D_{\text{source}_1}(t_{\text{end}}), D_{\text{source}_2}(t_{\text{end}})\}}{D(t_0)}, \quad (10)$$

where $D_{\text{source}_1}(t_{\text{end}})$ and $D_{\text{source}_2}(t_{\text{end}})$ represent the agent's distance to **source**₁ and **source**₂ at the end of the simulation. In multi-agent setups, performance is based on whether agents reach a consensus. Note that, in these experiments, an agent could no longer move once it came within 5 cm of a stimulus source, so any changes in agent angle and position due to agents circling around the stimulus source after arrival did not influence the decisions of the other agents. We evaluated performance based on the smallest average distance to one of the two stimulus sources:

$$\text{performance} = \min \left\{ \frac{1}{N} \sum_{n=1}^N \left[1 - \frac{D_{\text{source}_1}^n(t_{\text{end}})}{D(t_0)} \right], \frac{1}{N} \sum_{n=1}^N \left[1 - \frac{D_{\text{source}_2}^n(t_{\text{end}})}{D(t_0)} \right] \right\}, \quad (11)$$

with N being the number of agents and $D_{\text{source}_1}^n(t)$ being the Euclidean distance from **source**₁ to agent n at time t .

Measures of coordination dynamics

To evaluate the intra-agent neural dynamics, interagent neural dynamics, and interagent behavioral (i.e. movement) dynamics, we used the following measures: KOP (58), PLV (85), and wPLI (60).

First, we calculated KOP (i.e. the parameter $R(t)$ (58)) as

$$Z(t) = R(t)e^{i\phi} = \frac{1}{N} \sum_{i=1}^N e^{i\phi_i(t)}, \quad (12)$$

where N is the number of oscillators and ϕ_i is the phase angle of each oscillator (which, in this study, can be either the oscillator nodes of the neural controller or the movement directions of agents). KOP quantifies the extent to which several oscillating components are in phase. If KOP is 1, all components are completely in phase,

whereas low KOP values indicates an absence of synchronization between components. KOP values remaining constant over time indicate that the system has resorted to a stable dynamic (whether synchronized or not), whereas variation in the parameter indicate that the system is passing through various coordination states. Therefore, the standard deviation (SD) of KOP can be used as a measure of the metastability of coordination between oscillating components (59, 86). We used metastability to assess the agents' neural dynamics but also to evaluate the collective movements in the multiagent simulations. In the latter case, we used the measure of metastability to quantify the degree of "alignment variability," with which we mean the degree to which the collective switches between aligned and unaligned movement directions.

Based on (85), we calculated sliding PLV_{ij} for the connection between v_i and v_j as

$$\text{PLV}_{ij} = \frac{1}{T} \left| \sum_{t=1}^T e^{i\phi_{ij}(t)} \right|, \quad (13)$$

where T is the number of samples in a window. PLV is different from KOP in that it is maximal if the phases of the two oscillators are "locked," i.e. the relative phase of oscillators remains constant over time. We use PLV as a measure to indicate the degree of integration of the oscillating components, i.e. the degree to which their phases are co-determined. PLV is often used as a measure of connectivity between brain components (56) as well as functional connectivity between the brains of different individuals during social interaction (75).

Finally, wPLI_{ij} for the connection between v_i and v_j is calculated as follows (60):

$$\text{wPLI}_{ij} = \frac{\frac{1}{T} \left| \sum_{t=1}^T |I_{ij}(t)| \text{sgn}(I_{ij}(t)) \right|}{\frac{1}{T} \sum_{t=1}^T |I_{ij}(t)|}, \quad (14)$$

with

$$I_{ij}(t) = \text{Imag}(e^{i\phi_{ij}(t)}). \quad (15)$$

Like the PLV, the wPLI characterizes to what degree different oscillators are integrated (60) and has been used in several hyperscanning studies to quantify synchronization between brain regions (e.g. (62)). wPLI differs from PLV in that its weighting of phases puts more emphasis on the covariance of phases than simple "locking." When zero-phase locking (i.e. completely synchronized activity) driven by common input needs to be distinguished from locking between other phases, wPLI provides a more robust characterization of oscillator integration than PLV.

Acknowledgments

We thank Andreagiovanni Reina for useful suggestions to the manuscript. M.K. Heinrich, A. Cleeremans, and M. Dorigo acknowledge support from the F.R.S.-FNRS, of which they are, respectively, postdoctoral researcher and research directors.

Supplementary Material

Supplementary material is available at PNAS Nexus online.

Funding

This work was partially supported by the program of Concerted Research Actions (ARC) of the Université libre de Bruxelles and a Mitacs Globalink Research Award to N.C. This study was

supported by the Institute for Data Valorization, Montreal (IVADO; CF00137433 & PRF3) and enabled in part by support provided by Calcul Québec (www.calculquebec.ca) and Digital Research Alliance of Canada (www.alliancecan.ca). G.D. was supported by the Fonds de recherche du Québec - Santé (FRQ-S; 2024-2025 - CB - 350516), Natural Sciences and Engineering Research Council of Canada (NSERC; DGEER-2023-00089), the Brain Canada Foundation (2022 Future Leaders in Canadian Brain Research program), and the Azrieli Global Scholars Fellowship from the Canadian Institute for Advanced Research (CIFAR) in the Brain, Mind, & Consciousness program.

Author Contributions

N.C.: conceptualization, software, formal analysis, funding acquisition, investigation, visualization, methodology, writing—original draft, writing—review & editing; M.K.H.: supervision, formal analysis, writing—original draft, writing—review & editing; A.C.: supervision, funding acquisition, review & editing; M.D.: supervision, funding acquisition, project administration, writing—review and editing; G.D.: conceptualization, formal analysis, investigation, methodology, project administration, funding acquisition, writing—review & editing.

Preprints

This manuscript was posted on a preprint server: 10.48550/arXiv.2411.18498.

Data Availability

The code is available in an open-source code repository: <https://github.com/ppsp-team/PyHKBs>. There are no data underlying this work.

References

- Bang D, Frith CD. 2017. Making better decisions in groups. *R Soc Open Sci.* 4(8):170193.
- Conradt L, List C. 2008. Group decisions in humans and animals: a survey. *Philos Trans R Soc B.* 364(1518):719–742.
- Hamann H, Schmickl T, Wörn H, Crailsheim K. 2010. Analysis of emergent symmetry breaking in collective decision making. *Neural Comput Appl.* 21(2):207–218.
- Montes de Oca MA, et al. 2011. Majority-rule opinion dynamics with differential latency: a mechanism for self-organized collective decision-making. *Swarm Intell.* 5(3–4):305–327.
- Valentini G, Ferrante E, Dorigo M. 2017. The best-of- n problem in robot swarms: formalization, state of the art, and novel perspectives. *Front Robot AI.* 4:9.
- Couzin ID, et al. 2011. Uninformed individuals promote democratic consensus in animal groups. *Science.* 334(6062):1578–1580.
- Becker J, Brackbill D, Centola D. 2017. Network dynamics of social influence in the wisdom of crowds. *Proc Natl Acad Sci U S A.* 114:201615978.
- Centola D. 2022. The network science of collective intelligence. *Trends Cogn Sci.* 26(11):923–941.
- Couzin ID, Krause J, Franks NR, Levin SA. 2005. Effective leadership and decision-making in animal groups on the move. *Nature.* 433(7025):513–516.
- Bum Michael Yoo S, Yost Hayden B, Pearson JM. 2021. Continuous decisions. *Philos Trans R Soc B.* 376(1819):20190664.
- Suzuki S, Adachi R, Dunne S, Bossaerts P, O'Doherty JP. 2015. Neural mechanisms underlying human consensus decision-making. *Neuron.* 86(2):591–602.

- 12 Hegselmann R, Krause U. 2002. Opinion dynamics and bounded confidence models, analysis and simulation. *J Artif Soc Soc Simul.* 5(3).
- 13 Galam S. 2008. Sociophysics: a review of galam models. *Int J Mod Phys C.* 19(3):409–440.
- 14 Flache A, et al. 2017. Models of social influence: towards the next frontiers. *J Artif Soc Soc Simul.* 20(4):2.
- 15 Srivastava V, Ehrich Leonard N. 2014. Collective decision-making in ideal networks: the speed-accuracy tradeoff. *IEEE Trans Control Network Syst.* 1(1):121–132.
- 16 Tump AN, Pleskac TJ, Kurvers RHJM. 2020. Wise or mad crowds? The cognitive mechanisms underlying information cascades. *Sci Adv.* 6(29):eabb0266.
- 17 Lokesh R, et al. 2022. Humans utilize sensory evidence of others' intended action to make online decisions. *Sci Rep.* 12(1):8806.
- 18 Reina A, Bose T, Srivastava V, Marshall JAR. 2023. Asynchrony rescues statistically optimal group decisions from information cascades through emergent leaders. *R Soc Open Sci.* 10(3):230175.
- 19 Vicsek T, Czirók A, Ben-Jacob E, Cohen I, Shochet O. 1995. Novel type of phase transition in a system of self-driven particles. *Phys Rev Lett.* 75(6):1226–1229.
- 20 Helbing D, Molnar P. 1995. Social force model for pedestrian dynamics. *Phys Rev E.* 51(5):4282–4286.
- 21 Ma Y, Yuen RKK, Lee EWM. 2016. Effective leadership for crowd evacuation. *Phys A: Stat Mech Appl.* 450:333–341.
- 22 Reina A, Marshall James AR, Trianni V, Bose T. 2017. Model of the best-of-N nest-site selection process in honeybees. *Phys Rev E.* 95(5):052411.
- 23 Moussaïd M, Helbing D, Theraulaz G. 2011. How simple rules determine pedestrian behavior and crowd disasters. *Proc Natl Acad Sci U S A.* 108(17):6884–6888.
- 24 Kingsbury L, Hong W. 2020. A multi-brain framework for social interaction. *Trends Neurosci.* 43(9):651–666.
- 25 Moreau Q, Dumas G. 2021. Beyond “correlation vs. causation”: multi-brain neuroscience needs explanation. *Trends Cogn Sci.* 25(7):542–543.
- 26 Montserrat Reséndiz-Benhumea G, Sangati E, Sangati F, Keshmiri S, Froese T. 2021. Shrunk social brains? A minimal model of the role of social interaction in neural complexity. *Front Neurobot.* 15:634085.
- 27 Sridhar VH, et al. 2021. The geometry of decision-making in individuals and collectives. *Proc Natl Acad Sci U S A.* 118(50):e2102157118.
- 28 Heins C, et al. 2024. Collective behavior from surprise minimization. *Proc Natl Acad Sci U S A.* 121(17):e2320239121.
- 29 Clark A. *Being there.* The MIT Press, 1998.
- 30 Newen A, Gallagher S. *The oxford handbook of 4E cognition.* Oxford University Press, 2018.
- 31 Steels L, Brooks R. *The artificial life route to artificial intelligence: building embodied, situated agents.* Routledge, 2018.
- 32 Colas C, Karch T, Moulin-Frier C, Oudeyer P-Y. 2022. Language and culture internalization for human-like autotelic AI. *Nat Mach Intell.* 4(12):1068–1076.
- 33 Varela FJ, Thompson ET, Rosch E. *The embodied mind.* The MIT Press, 1992.
- 34 Thompson E, Varela FJ. 2001. Radical embodiment: neural dynamics and consciousness. *Trends Cogn Sci.* 5(10):418–425.
- 35 Froese T, Di Paolo EA. 2011. The enactive approach. *Pragmat Cogn.* 19(1):1–36.
- 36 Ward LM. 2003. Synchronous neural oscillations and cognitive processes. *Trends Cogn Sci.* 7(12):553–559.
- 37 Buzsáki G. *The brain from inside out.* Oxford University Press, 2019.
- 38 Buzsáki G, Logothetis N, Singer W. 2013. Scaling brain size, keeping timing: evolutionary preservation of brain rhythms. *Neuron.* 80(3):751–764.
- 39 Senoussi M, et al. 2022. Theta oscillations shift towards optimal frequency for cognitive control. *Nat Hum Behav.* 6(7):1000–1013.
- 40 Charalambous E, Djebbara Z. 2023. On natural attunement: shared rhythms between the brain and the environment. *Neurosci Biobehav Rev.* 155(10):105438.
- 41 Scott Kelso JA. *Dynamic patterns the self-organization of brain and behavior.* Bradford Book, 1997.
- 42 Scott Kelso JA, Tognoli E, Dumas G. Coordination dynamics: bidirectional coupling between humans, machines and brains. In 2014 IEEE International Conference on Systems, Man, and Cybernetics (SMC). IEEE, 2014. <https://doi.org/10.1109/smc.2014.6974258>
- 43 Tognoli E, Zhang M, Fuchs A, Beetle C, Scott Kelso JA. 2020. Coordination dynamics: a foundation for understanding social behavior. *Front Hum Neurosci.* 14:317.
- 44 Tognoli E, Scott Kelso JA. 2014. The metastable brain. *Neuron.* 81(1):35–48.
- 45 Haken H, Scott Kelso JA, Bunz H. 1985. A theoretical model of phase transitions in human hand movements. *Biol Cybern.* 51(5):347–356.
- 46 Kuramoto Y. *Chemical oscillations, waves, and turbulence.* Springer, Berlin, 1984.
- 47 Scott Kelso JA. Coordination dynamics. 2013. In *Encyclopedia of complexity and systems science.* New York (NY): Springer. p. 1–41. https://doi.org/10.1007/978-3-642-27737-5_101-3
- 48 Aguilera M, Bedia MG, Santos BA, Barandiaran XE. 2013. The situated HKB model: how sensorimotor spatial coupling can alter oscillatory brain dynamics. *Front Comput Neurosci.* 7:117.
- 49 Leonard NE, et al. 2011. Decision versus compromise for animal groups in motion. *Proc Natl Acad Sci U S A.* 109(1):227–232.
- 50 Lloyd JE, Wing SR. 1983. Nocturnal aerial predation of fireflies by light-seeking fireflies. *Science.* 222(4624):634–635.
- 51 Fernandes AM, et al. 2012. Deep brain photoreceptors control light-seeking behavior in zebrafish larvae. *Curr Biol.* 22(21):2042–2047.
- 52 Braitenberg V. *Vehicles, experiments in synthetic psychology.* MIT Press, 1986.
- 53 Zhang M, Beetle C, Scott Kelso JA, Tognoli E. 2019. Connecting empirical phenomena and theoretical models of biological coordination across scales. *J R Soc Interface.* 16(157):20190360.
- 54 Schafer Edward WP, Marcus MM. 1973. Self-stimulation alters human sensory brain responses. *Science.* 181(4095):175–177.
- 55 Crapse TB, Sommer MA. 2008. Corollary discharge across the animal kingdom. *Nat Rev Neurosci.* 9(8):587–600.
- 56 Varela F, Lachaux J-P, Rodriguez E, Martinerie J. 2001. The brain-web: phase synchronization and large-scale integration. *Nat Rev Neurosci.* 2(4):229–239.
- 57 Avena-Koenigsberger A, Misic B, Sporns O. 2018. Communication dynamics in complex brain networks. *Nat Rev Neurosci.* 19(1):17–33.
- 58 Strogatz SH. 2000. From Kuramoto to Crawford: exploring the onset of synchronization in populations of coupled oscillators. *Phys D: Nonlinear Phenom.* 143(1–4):1–20.
- 59 Cabral J, et al. 2022. Metastable oscillatory modes emerge from synchronization in the brain spacetime connectome. *Commun Phys.* 5(1):184.
- 60 Vinck M, Oostenveld R, van Wingerden M, Battaglia F, Pennartz Cyriel MA. 2011. An improved index of phase-synchronization for electrophysiological data in the presence of volume-conduction, noise and sample-size bias. *Neuroimage.* 55(4):1548–1565.

- 61 Czeszumski A, et al. 2020. Hyperscanning: a valid method to study neural inter-brain underpinnings of social interaction. *Front Hum Neurosci.* 14:39.
- 62 Schwartz L, et al. 2022. Technologically-assisted communication attenuates inter-brain synchrony. *Neuroimage.* 264(1-2):119677.
- 63 Waller J. *A time to dance, a time to die.* Icon Books, 2008.
- 64 Couzin ID, Franks NR. 2003. Self-organized lane formation and optimized traffic flow in army ants. *Proc R Soc London, B.* 270(1511):139–146.
- 65 Valentini G, Ferrante E, Hamann H, Dorigo M. 2015. Collective decision with 100 Kilobots: speed versus accuracy in binary discrimination problems. *Auton Agents Multi-Agent Syst.* 30(3): 553–580.
- 66 Hölldobler B, Wilson EO. *The ants.* Belknap Press, 1990.
- 67 Theraulaz G, Bonabeau E. 1999. A brief history of stigmergy. *Artif Life.* 5(2):97–116.
- 68 Pickavance J, Azmoodeh A, Wilson AD. 2018. The effects of feedback format, and egocentric & allocentric relative phase on coordination stability. *Hum Mov Sci.* 59(1):143–152.
- 69 Bonabeau E, Dorigo M, Theraulaz G. *Swarm intelligence.* Oxford University Press Inc, 1999.
- 70 Kahneman D, Krakauer DC, Sibony O, Sunstein C, Wolpert D. 2022. An exchange of letters on the role of noise in collective intelligence. *Collective Intell.* 1(1):263391372210785.
- 71 O’Keeffe KP, Hong H, Strogatz SH. 2017. Oscillators that sync and swarm. *Nat Commun.* 8(1):1504.
- 72 Ceron S, O’Keeffe K, Petersen K. 2023. Diverse behaviors in non-uniform chiral and non-chiral swarmalators. *Nat Commun.* 14(1):940.
- 73 Auvray M, Lenay C, Stewart J. 2009. Perceptual interactions in a minimalist virtual environment. *New Ideas Psychol.* 27(1):32–47.
- 74 De Jaegher H, Di Paolo E, Gallagher S. 2010. Can social interaction constitute social cognition? *Trends Cogn Sci.* 14(10):441–447.
- 75 Dumas G, Nadel J, Soussignan R, Martinerie J, Garnero L. 2010. Inter-brain synchronization during social interaction. *PLoS One.* 5(8):e12166.
- 76 Yang Y, et al. 2021. Wireless multilateral devices for optogenetic studies of individual and social behaviors. *Nat Neurosci.* 24(7): 1035–1045.
- 77 Dumas G, Chavez M, Nadel J, Martinerie J. 2012. Anatomical connectivity influences both intra- and inter-brain synchronizations. *PLoS One.* 7(5):e36414.
- 78 Moreau Q, Adel L, Douglas C, Ranjbaran G, Dumas G. 2022. A neurodynamic model of inter-brain coupling in the gamma band. *J Neurophysiol.* 128(5):1085–1090.
- 79 Adrian Heggli O, Cabral J, Konvalinka I, Vuust P, Kringelbach ML. 2019. A Kuramoto model of self-other integration across interpersonal synchronization strategies. *PLoS Comput Biol.* 15(10):e1007422.
- 80 Bolotta S, Dumas G. 2022. Social neuro AI: social interaction as the “Dark Matter” of AI. *Front Comput Sci.* 4:846440.
- 81 Van Rossum G, Drake FL. *Python 3 reference manual.* CreateSpace, Scotts Valley, CA, 2009.
- 82 Paszke A, et al. Pytorch: an imperative style, high-performance deep learning library. In: *Advances in neural information processing systems* 32. Curran Associates, Inc., 2019. p. 8024–8035. <http://papers.neurips.cc/paper/9015-pytorch-an-imperative-style-high-performance-deep-learning-library.pdf>.
- 83 Sterling P, Laughlin S. *Principles of neural design.* The MIT Press, 2017.
- 84 Nabet B, Leonard NE, Couzin ID, Levin SA. 2009. Dynamics of decision making in animal group motion. *J Nonlinear Sci.* 19(4): 399–435.
- 85 Lachaux J-P, Rodriguez E, Martinerie J, Varela FJ. 1999. Measuring phase synchrony in brain signals. *Hum Brain Mapp.* 8(4):194–208.
- 86 Shanahan M. 2010. Metastable chimera states in community-structured oscillator networks. *Chaos.* 20(1):013108.